

## SUPPORTING INFORMATION

### **A Benzimidazole based non-symmetrical tripodal receptor for ratiometric fluorescent sensing of fluoride ions and solid state recognition of sulfate ions**

Nilotpall Borah, Biswajit Nayak, Abhijit Gogoi, and Gopal Das\*

*Department of Chemistry, Indian Institute of Technology Guwahati, Assam-  
781039, India Fax: +91-361-2582349; Tel: +91-361-2582313;*

*E-mail: gdas@iitg.ac.in*

## Experimental

### Materials and measurements

All of the reagents and solvents were commercially available and used henceforth. Perkin-Elmer Lambda-25 UV-Vis spectrophotometer was used to achieve the absorption spectra which were recorded using quartz cuvette of path length 10 mm in the range 250–450 nm wavelengths. The emission spectra were obtained through a Horiba Fluoromax-4 spectrofluorometer. The mass spectra of **L** were obtained using an Agilent Technologies 6520 Accurate mass spectrometer. The infrared spectra were recorded on a Perkin-Elmer Spectrum One FT-IR spectrometer with KBr pellets in the range 4000–400  $\text{cm}^{-1}$ . NMR spectra were recorded and documented on a Varian FT-400 MHz and a Bruker 600 MHz instruments. Parts per million (ppm) were used to represent the chemical shifts value on the delta scale. The abbreviated vocabularies were used to describe spin multiplicities in  $^1\text{H}$ NMR spectra viz. ‘s’ for singlet; ‘d’ for doublet; ‘t’ for triplet; ‘m’ for multiplet.

### Study of Optical properties of the probe **L**

For UV-vis study, stock solutions of the receptor and the other ions were prepared independently. The stock solution of **L** ( $5 \times 10^{-3} \text{ mol L}^{-1}$ ) was prepared in DMSO while the stock solutions of different anions ( $50 \times 10^{-3} \text{ mol L}^{-1}$ ) were prepared in acetonitrile using their corresponding tetrabutyl/tetraethyl or sodium salts. For fluorescence titration, a similar concentration of the receptor, as well as anion solutions, were followed and prepared separately. Emission spectra were recorded with  $\lambda_{\text{ex}} = 285 \text{ nm}$  using quartz cuvettes of 10 mm path length with a slit width of 3 nm at 298 K. For the competition study, emission spectra of the receptor **L** with were recorded individually in the presence of  $\text{F}^-$  and other anions. An effective concentration of 10.0  $\mu\text{M}$  receptor **L** was used for the

emission titration studies with  $F^-$  solution while varying concentration between 0 and 60  $\mu\text{M}$  were taken as the effective  $F^-$  concentrations for the titration studies. Job's plot was achieved using fluorescence emission measurements. The detection limit (LOD) was estimated based on the fluorescence titration.

### **Single-crystal structure determination**

A suitable crystal for single crystal determination was selected carefully from the mother liquor. After being immersed in silicone oil, the appropriate sized crystal was selected. With the help of epoxy resin, it was attached to the tip of a glass fiber and cemented. Bruker SMART APEX II CCD diffractometer fortified with Mo- $K\alpha$  radiation ( $\lambda = 0.71073 \text{ \AA}$ ) at 298 K were used to collect the intensity data. SAINT and XPREP software<sup>1</sup> were employed for crystal data integration and reduction. Corrections related to Multi-scan empirical absorption were applied to the data using the program SADABS<sup>2</sup>. Crystal structures resolution were carried out by direct methods using SHELXTL-2014 and were subjected to refinement on  $F^2$  by the full matrix least-squares technique using the SHELXL-2014 program.<sup>3</sup> Structural illustrations of the crystal structures were created using MERCURY 4.0 for Windows.

### **The synthesis of 1,1-bis((1H-benzo[d]imidazol-2-yl)methyl)-3-(naphthalen-1-yl)urea, L**

Initially, 1-Naphthyl isocyanate (338 mg, 2 mmol) was refluxed and stirred with previously reported ligand Bis(2-benzimidazolylmethyl) amine<sup>4</sup> (554 mg, 2 mmol) in dry DCM for 24 hours maintaining a molar ratio of 1:1. Evaporation of the brown coloured solution and work up with  $\text{CHCl}_3/\text{H}_2\text{O}$  yields the receptor L, 1,1-bis((1H-benzo[d]imidazol-2-yl)methyl)-3-(naphthalen-1-yl)urea. The compound was finally dried in vacuum over silica gel. The product L was

obtained as brown coloured solid with a yield of 75% (Scheme 1, Main article). Later it was recrystallized from DMSO-MeOH (2:3) mixture and left for slow evaporation. Red block type crystal were obtained after 4-5 weeks which are appropriate for X-ray analysis.  $^1\text{H}$  NMR (600 MHz, DMSO- $d_6$ )  $\delta$  (ppm): 13.02 (s, 2H, Benzimidazole-NH), 9.28 (s, 1H, amide -NH), 8.17-8.16 (d, 1H, ~8.4 Hz, Ar<sub>H</sub>), 7.88-7.87 (d, 1H, ~8.4 Hz, Ar<sub>H</sub>), 7.73-7.71 (d, 2H, ~6 Hz, Ar<sub>H</sub>), 7.68-7.67 (d, 1H, ~7.8 Hz, Ar<sub>H</sub>), 7.60-7.57 (m, 3H, Ar<sub>H</sub>), 7.48-7.43 (m, 2H, Ar<sub>H</sub>), 7.39-7.37 (t, 1H, ~7.8 Hz, Ar<sub>H</sub>), 7.23-7.22 (d, 4H, ~6 Hz, Ar<sub>H</sub>), 5.04 (s, 4H, aliphatic -CH<sub>2</sub>).  $^{13}\text{C}$  NMR (100 MHz, DMSO- $d_6$ )  $\delta$  (ppm): 156.85, 152.99, 135.64, 134.17, 128.66, 128.42, 126.24, 125.99, 125.87, 124.72, 123.65, 121.56 and 46.61 FTIR (KBr pellet,  $\text{cm}^{-1}$ ): 3243 (N-H), 3049 (C-H<sub>alp</sub>), 1645 (C=O), 1515 (C=C), 1448 (C=C), 1274 (C-N); ESI m/z: 447.50 (calculated 446.50).

#### **Preparation of anion complex $[2(\text{LH}_2)^{2+} \cdot 2\text{SO}_4^{2-}]$ :**

In 5 mL DMSO, 0.067 g (0.15 mmol), the receptor **L** was added and solubilized. After addition of 4-6 drops (0.5 mL) of concentrated H<sub>2</sub>SO<sub>4</sub>, the clear blue coloured solution was kept under stirring for 1 hour. The solution was filtered out and allowed for slow evaporation at room temperature in a glass vial. Slow evaporation of the solvent mixture afforded blue coloured block like small crystal after 8-10 weeks which were suitable for X-ray analysis. Yield: 75-80%.  $^1\text{H}$  NMR (400 MHz, DMSO- $d_6$ )  $\delta$  (ppm): 9.20 (s, amide -NH), 7.88-7.84 (m, 6H, Ar<sub>H</sub>), 7.73-7.71 (d, 1H, ~7.6 Hz, Ar<sub>H</sub>), 7.45-7.38 (m, 7H, Ar<sub>H</sub>), 7.31-7.27 (t, 1H, Ar<sub>H</sub>), 5.30 (s, 4H, ~7.6 Hz aliphatic -CH<sub>2</sub>). IR (KBr pellet,  $\text{cm}^{-1}$ ): 3330 (N-H), 3058 (C-H alp), 1672 (C=O), 1520 (C=C), 1462 (C=C), 1119 (S=O).

#### **Characterization of receptor **L**:**

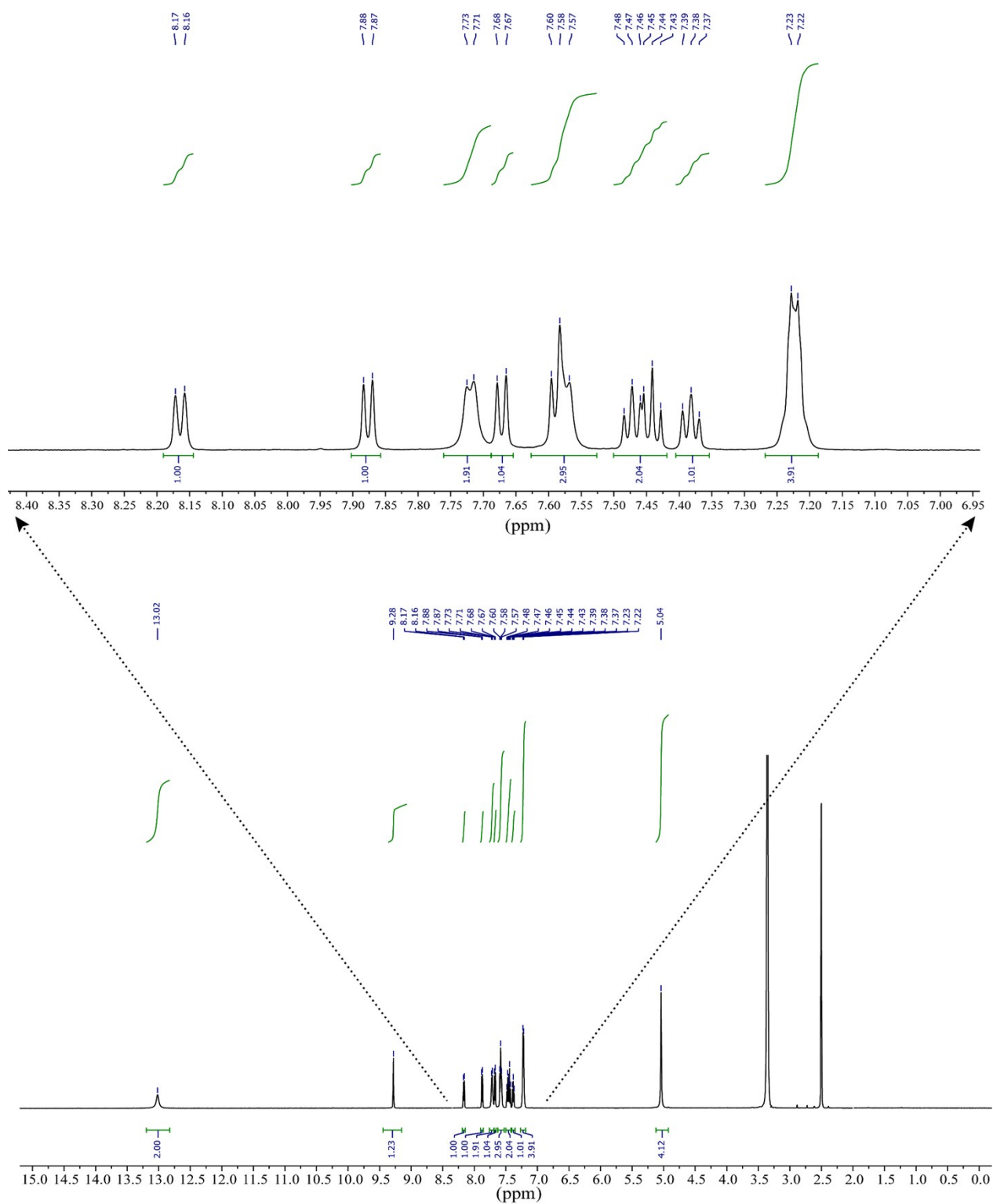


**Figure S1.** Integrated  $^1\text{H-NMR}$  spectrum (full as well as expanded) of free receptor **L** in  $\text{DMSO-d}_6$  at 298 K.

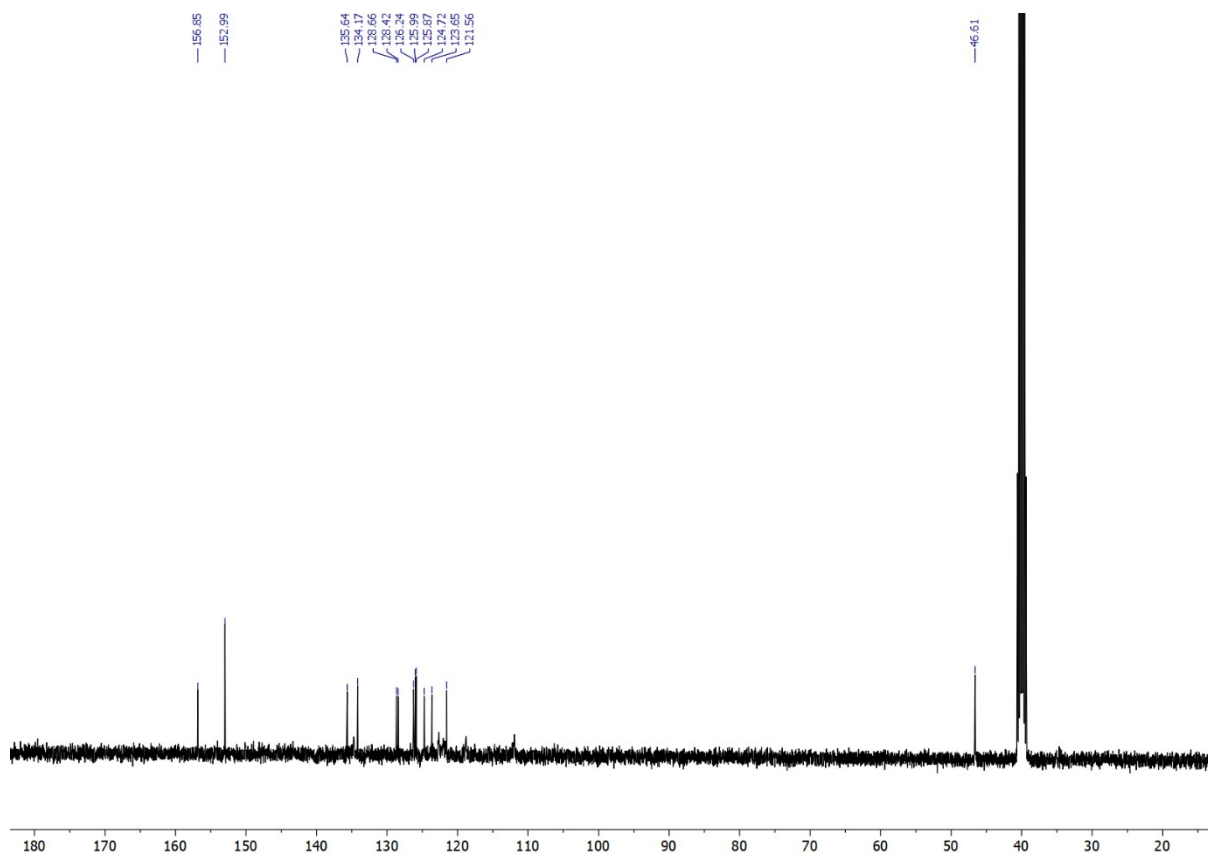


**Figure S2:**  $^{13}\text{C}$ -NMR spectrum of free receptor L in DMSO- $\text{d}_6$  at 298 K.

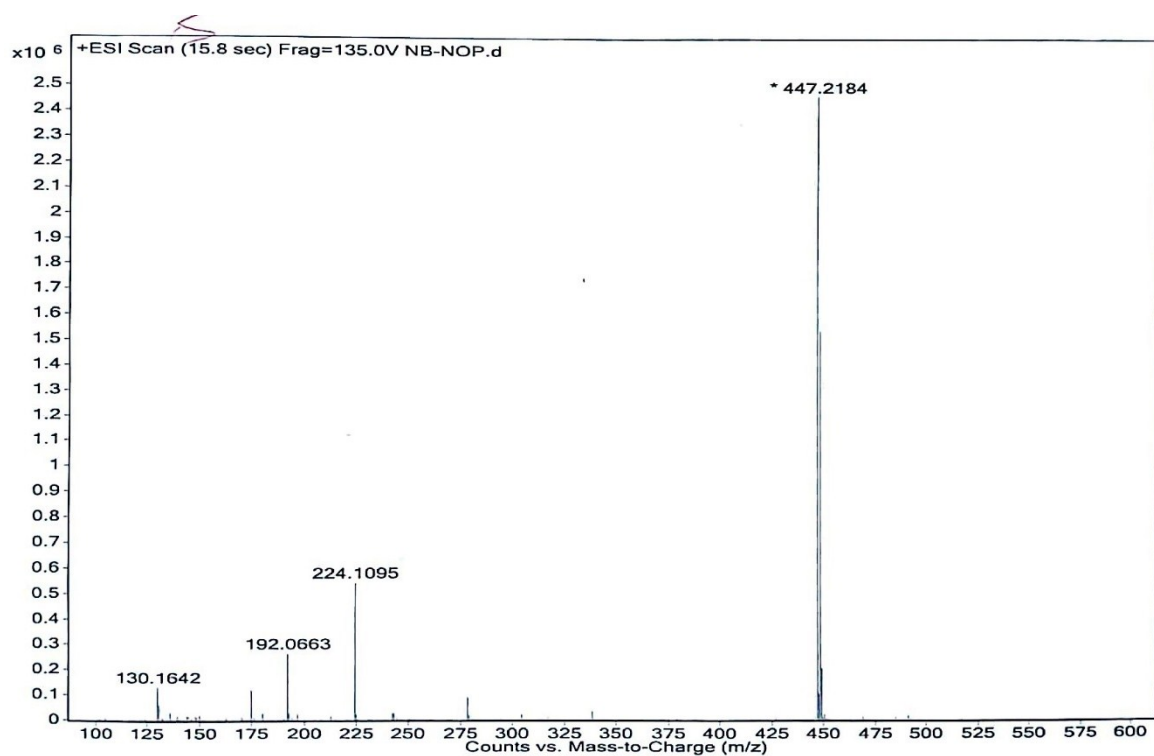


**Figure S3.** ESI-Mass spectrum of receptor L in acetonitrile.

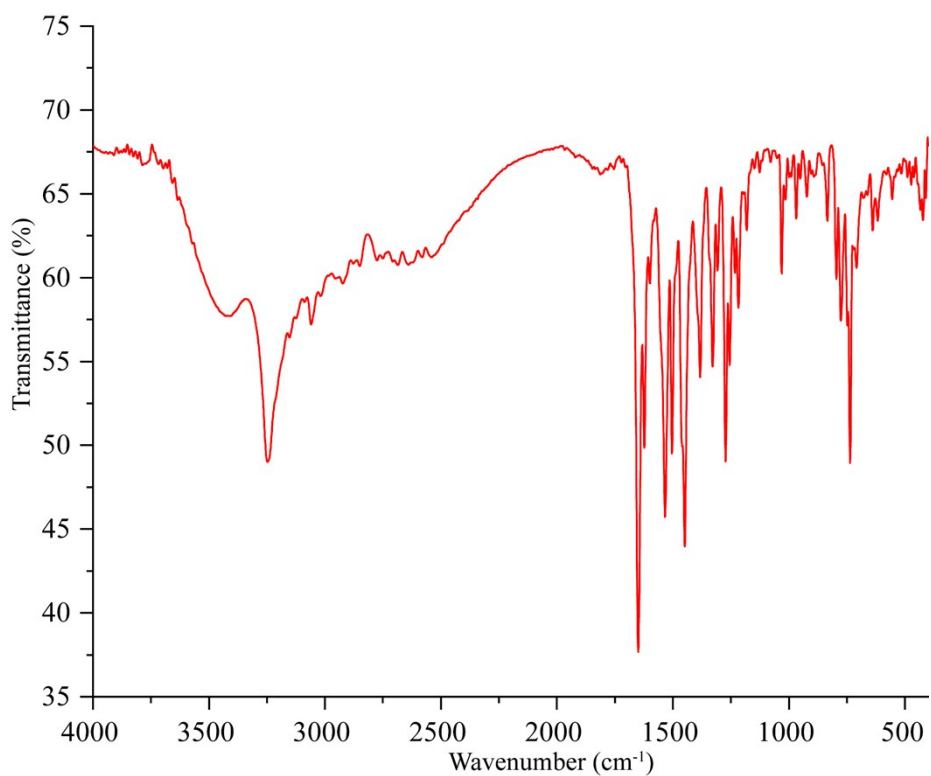


**Figure S4.** FT-IR spectrum (KBr pellet) of the receptor **L**.

**Characterization of protonated anion complex of receptor:**

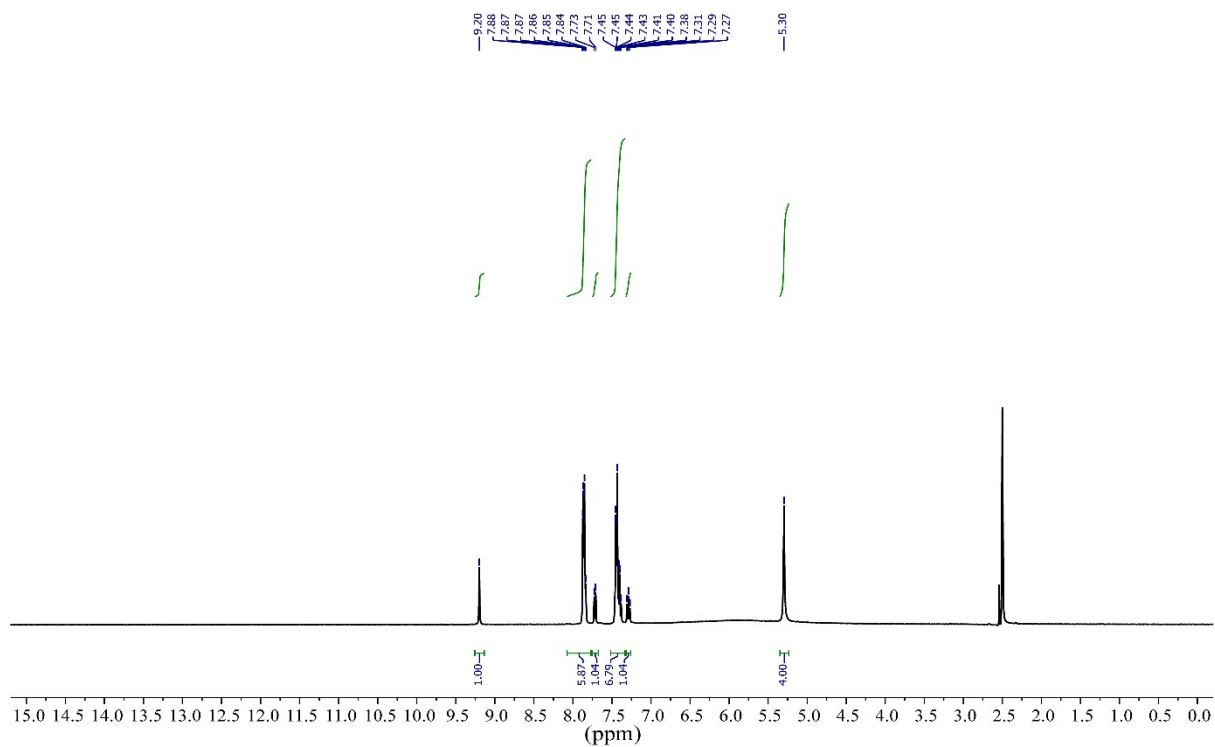


**Figure S5.**  $^1\text{H}$  NMR spectrum (400 MHz,  $\text{DMSO-d}_6$ , 298 K) of complex **1**  $[2(\text{LH}_2)^{2+} \cdot 2\text{SO}_4^{2-}]$

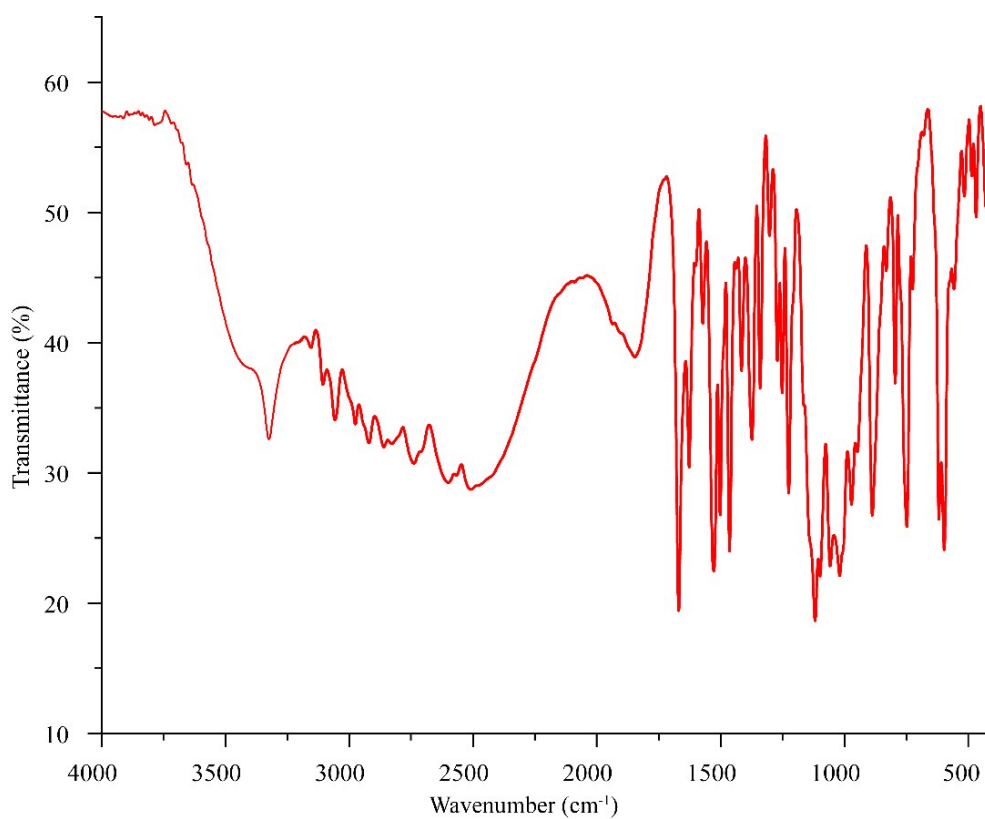


**Figure S6.** FT-IR spectrum (KBr pellet) of the complex **1**  $[2(\text{LH}_2)^{2+} \cdot 2\text{SO}_4^{2-}]$

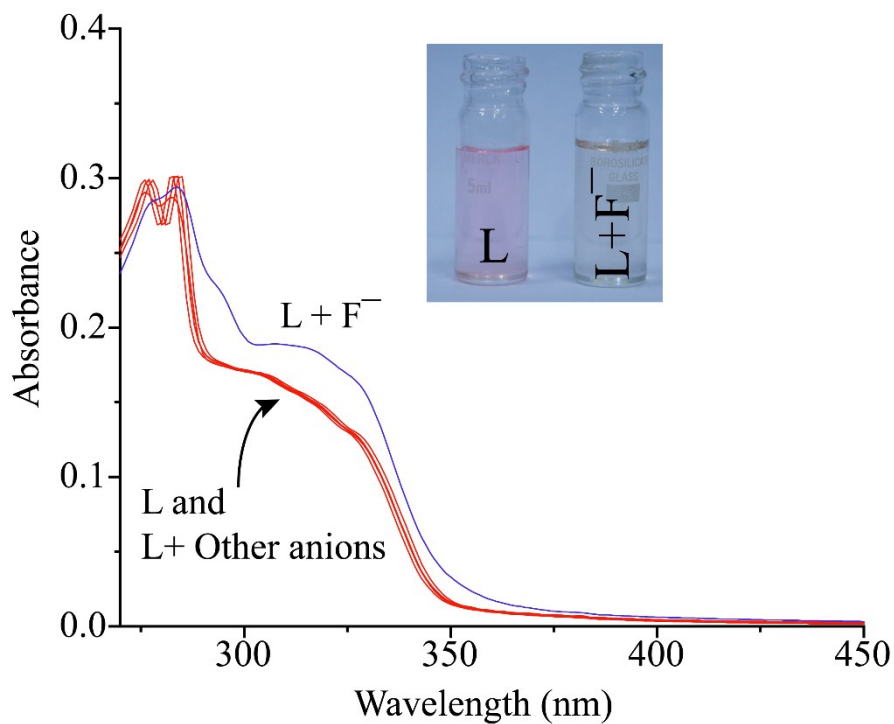


**Figure S7.** (a) Change in absorption spectra of **L** (10 mM) with different anions (50 mM) in acetonitrile solution. Inset: Corresponding change in the colour of the probe solution after the addition of  $\text{F}^-$ .

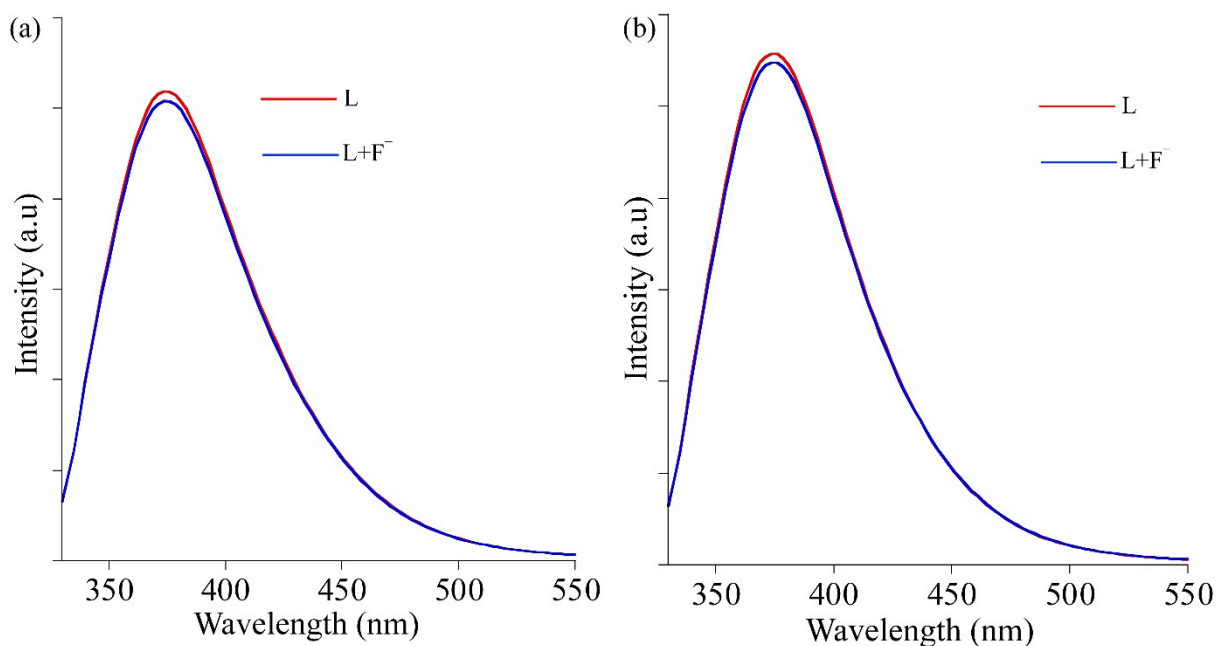


**Figure S8.** (a) Change in emission spectra of **L** (10 mM) with fluoride anion (50 mM) in (a) Acetonitrile: H<sub>2</sub>O=9:1 (b) Acetonitrile: H<sub>2</sub>O=4:1 solution.

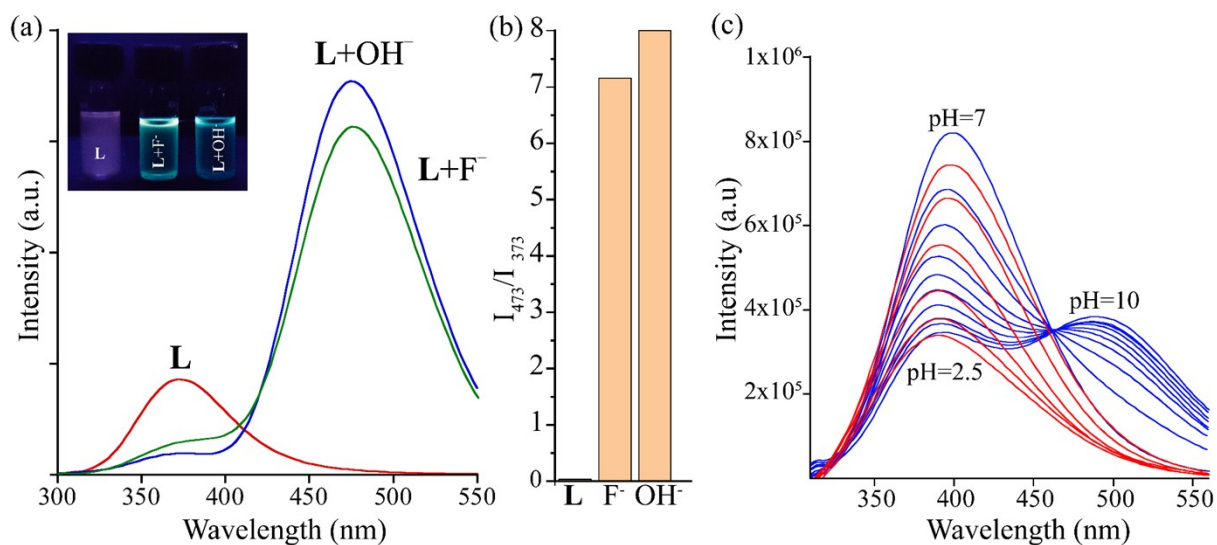


**Figure S9.** (a) The comparative emission spectra of TBOH and TBAF addition to the receptor **L** in acetonitrile. Inset: Visible colour change upon addition of the two anions F<sup>-</sup> and OH<sup>-</sup> under UV lamp ( $\lambda_{\text{ex}} = 365 \text{ nm}$ ). (b) Relative fluorescence intensity ratio  $I_{473}/I_{373}$  upon the addition of 10 equivalents of F<sup>-</sup> and OH<sup>-</sup> anions. (c) Change of the fluorescence spectra of **L** (5 mM) with decreasing pH from 10 to 2.5 ( $\lambda_{\text{ex}} = 285 \text{ nm}$ ) in aqueous medium.

## Determination of stoichiometry by Job's plot and plotting of B-H plot:

Job plots were achieved using fluorescence emission measurements.  $\Delta I \cdot X_h$  versus  $X_h$  was plotted where  $\Delta I$  is the change in emission intensity during titration and  $X_h$  is the mole fraction of host in the solution. The apparent binding constants for the formation of the respective complexes are evaluated using the Benesi–Hildebrand (B–H) plot (eqn (1)).<sup>5-7</sup>

$$1/(I-I_0)=1/\{K(I_{max}-I_0)C^3\}+1/(I_{max}-I_0) \quad (1)$$

$I_0$  is the emission intensity of L at  $\lambda=473$  nm for  $F^-$  ion,  $I$  is the observed emission intensity at the particular wavelength in the presence of a certain concentration of the anion ( $C$ ),  $I_{max}$  is the maximum emission intensity value that was obtained at  $\lambda=473$  nm during titration with varying metal ion concentration,  $K$  is the apparent binding constant ( $M^{-1}$ ) which was calculated from the slope of the linear plot, and  $C$  is the concentration of the added  $F^-$  ion during titration.

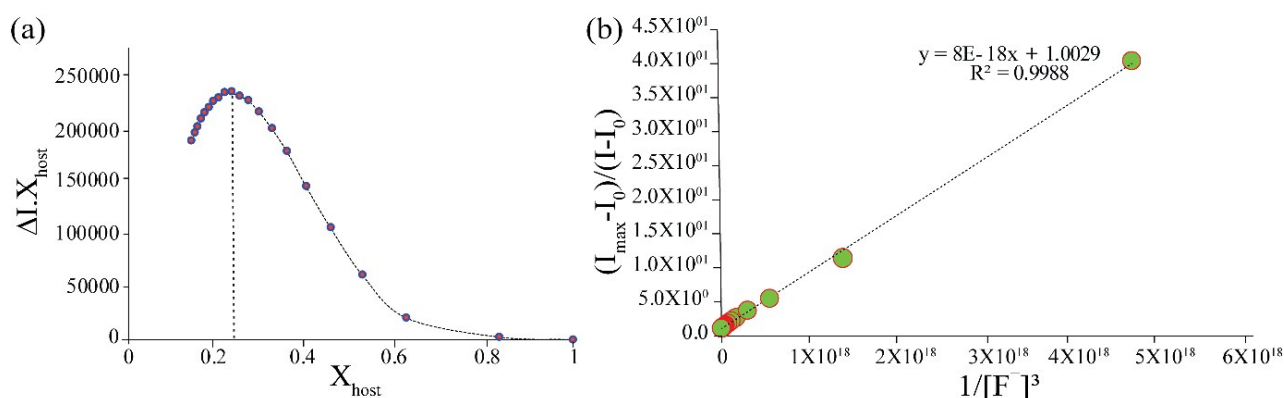


**Figure S10.** (a) Job's plot for determining the stoichiometry of the probe and  $F^-$  ion and (b) the corresponding Benesi–Hildebrand plot for binding constant determination.

### Calculations for detection limit:

A continuous measurement of emission spectrum of the probe L was carried out 10 times and the standard deviation of blank measurement was determined. To gain the slope, the ratio of the fluorescence emission at 473 nm was plotted against the concentration of added  $F^-$  ion. The detection limit (LOD) of probe L for  $F^-$  were determined from the following equation:

$$LOD = 3\sigma/k \quad (2)$$

$\sigma$  is the standard deviation of the blank solution which is found to be 6174.

$k$  is the slope of the calibration curve i.e.  $4 \times 10^{11}$

Hence detection limit =  $4.63 \times 10^{-8} \text{M}$  OR 0.463 nM or 0.875 ppb.

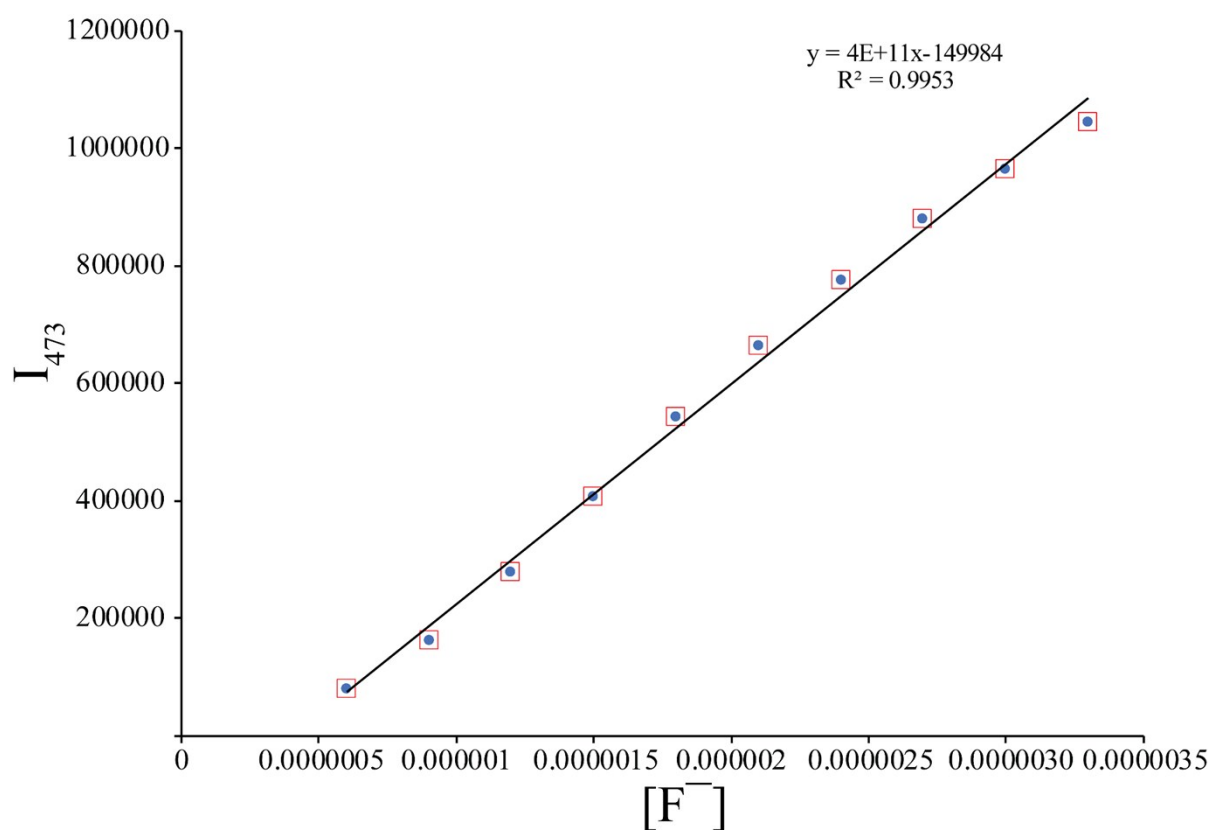


**Figure S11.** Ratio of fluorescence emission intensity change at 473 nm versus concentrations for lowest detection limits (LOD) calculation.

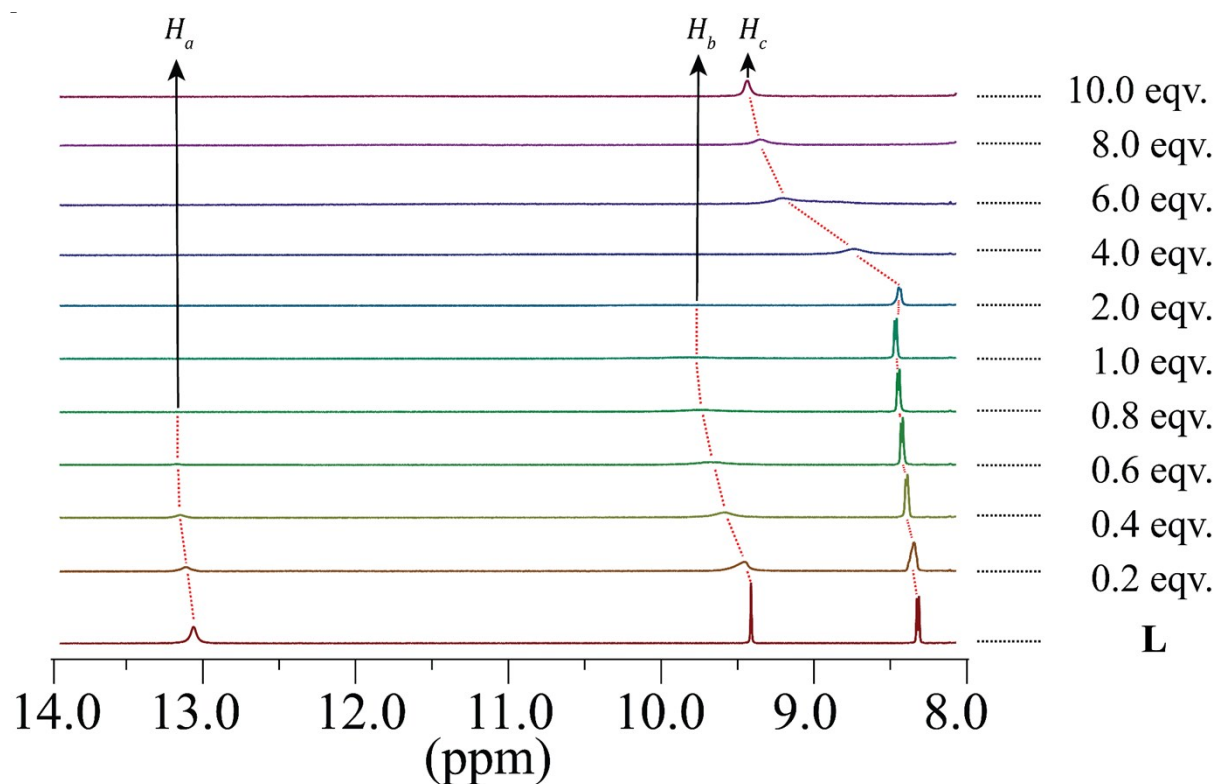


**Figure S12.** Enhanced view (8–14ppm) of stack plot of  $^1\text{H}$  NMR spectra of receptor **L** in the presence of increasing amounts of TBAF (1–10 equiv.) recorded in  $\text{DMSO-d}_6$ .

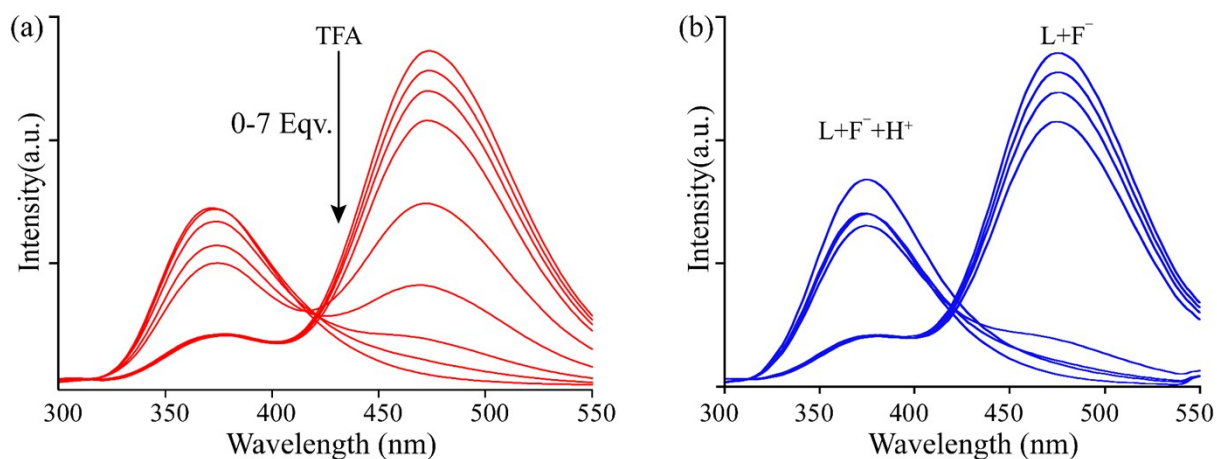


**Figure S13.** (a) Titration of L-  $F^-$  complex with Trifluoroacetic acid. (b) Reversibility test of the probe: Ratiometric shift of 100nm with the addition of fluoride ions ( $F^-$ ) and reversed back to the original upon addition of TFA.

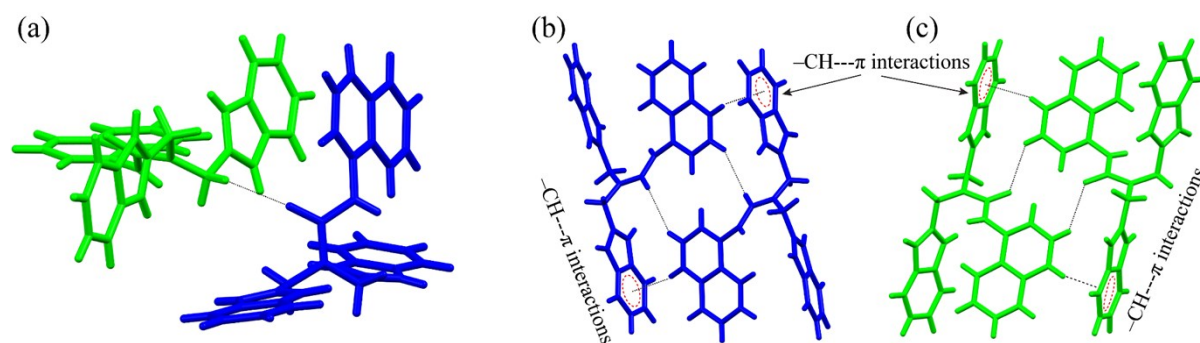


**Figure S14.** (a) The interacting isomorphs represented in different colors (blue = C1, green = C2). The  $-CH$  (aliphatic)  $\cdots \pi$  interactions and  $-CH$  (aromatic)  $\cdots$  amide  $C=O$  interactions extending the (b) C1 chain and (c) C2 chain.

**Table S1: Crystallographic data and refinement details.**

<b>Formula</b>	<b>C<sub>27</sub> H<sub>22</sub> N<sub>6</sub> O</b>	<b>C<sub>27</sub> H<sub>24</sub> N<sub>6</sub> O<sub>5</sub> S</b>
CCDC	1920832	1920833
Fw	446.51	544.58
Crystal system	triclinic	triclinic
Space group	<i>P</i> -1	<i>P</i> -1
a/Å	11.3681(7)	12.349(4)
b/Å	14.1597(10)	13.224(4)
c/Å	15.0368(9)	16.924(6)
α/°	82.533(3)	99.628(12)
β/°	76.926(3)	108.857(11)
γ/°	77.221(3)	90.120(11)
V/Å <sup>3</sup>	2291.2(3)	2573.9(14)
Z	4	4
D <sub>c</sub> /(g cm <sup>-3</sup> )	1.294	1.405
μ (Mo K <sub>α</sub> )/mm <sup>-1</sup>	0.083	0.177
T/K	298(2)	298(2)
θ max.	28.95	20.28
Total no. of reflections	40988	91599
Independent reflections	12256	9080
Observed reflections	8485	567
Parameters refined	614	704
R <sub>1</sub> , I > 2σ(I)	0.0772	0.1529
wR <sub>2</sub> (all data)	0.2312	0.3318
GOF (F <sup>2</sup> )	0.997	1.800

**Table S2:** Hydrogen bonding distances (Å) and Bond angles (°) in the receptor crystal

D–H...A	d(D...H)/Å	d(H...A)/Å	d(D...A)/Å	<D–H...A/°	Symmetry codes
N1-H3...N4	0.860	2.232	2.944	140.12	[ -x, -y, -z+1 ]
N3-H3N...N5	0.860	1.967	2.791	160.12	x,y,z
N5-H5N...N3	0.860	1.940	2.791	170.18	x,y,z
N7-H24...N11	0.860	2.222	2.971	145.64	[ -x+2, -y, -z ]
N9-H26...O1	0.860	1.992	2.788	153.45	x,y,z
N12-H12N...N10	0.860	1.947	2.796	169.00	x,y,z
C12-H9...N4	0.970	2.660	3.540	151.13	[ -x, -y, -z+1 ]

**Table S3:** Hydrogen bonding distances (Å) and Bond angles (°) in the protonated complex

D–H...A	d(D...H)/Å	d(H...A)/Å	d(D...A)/Å	<D–H...A/°	Symmetry codes
N1--H1N...O3	0.86	1.87	2.699(8)	163	x,y,z
N2--H2N...O8	0.86	1.82	2.665(8)	168	[ -x, 1-y, 1-z ]
N4--H4N...O5	0.86	1.84	2.672(8)	163	[ 1-x, -y, 1-z ]
N5--H5N...O7	0.86	1.85	2.679(8)	163	x,y,z
N6--H6N...O4	0.86	2.22	3.035(8)	158	[ 1-x, -y, 1-z ]
N7--H7N...O5	0.86	1.83	2.668(8)	163	[ 1-x, -y, 1-z ]
N8--H8N...O7	0.86	1.81	2.650(8)	165	[ 1+x, y, z ]
N10--H10N...O4	0.86	1.82	2.678(8)	171	[ x, y, z ]
N11--H11N...O9	0.86	1.86	2.696(8)	164	[ 1-x, 1-y, 1-z ]
N12--H12N...O8	0.86	2.24	3.052(8)	157	[ 1+x, y, z ]
Intra C14--H14...O2	0.93	2.48	2.896(10)	108	x,y,z
Intra C01--H1...N12	0.93	2.57	2.879(10)	100	x,y,z
C2--H2...O10	0.93	2.59	3.387(11)	144	[ -x, 1-y, 1-z ]
C5--H5...O6	0.93	2.43	3.264(11)	150	x,y,z
C8--H8A...O7	0.97	2.43	3.141(8)	130	x,y,z
C9--H9B...O2	0.97	2.28	2.956(9)	126	x,y,z
Intra C19--H19...O1	0.93	2.45	2.871(9)	108	x,y,z
C29--H29...O6	0.93	2.59	3.464(12)	156	[ 1-x, -y, 1-z ]
C35--H35B...O1	0.97	2.32	2.976(9)	124	[ 1+x, y, z ]
C36--H36A...O5	0.97	2.44	3.147(9)	129	[ 1-x, -y, 1-z ]
C39--H39...O10	0.93	2.46	3.274(11)	147	[ 1-x, 1-y, 1-z ]

**Table S4.** The comparison of our chemosensors L with F<sup>-</sup> sensors available in recent literatures.

No.	Chemosensor type	Solvent	Reversibility and reusability	Detection limit	Ref.
1	BODIPY-benzimidazole	CH <sub>3</sub> CN	Yes	0.093 μM	8
2	Pyrene-benzimidazole	DMSO	Yes	1.63 × 10 <sup>-5</sup> M	9
3	1,2-dioxetane derivative	DMSO	No	47 μM	10
4	7-(diethylamino)-3-(2-(pyridin-4-yl)vinyl)-coumarin and triisopropylsilane ether	DMSO:PBS (7:3)	No	1.2 × 10 <sup>-8</sup> M	11
5	BN-Embedded phenacenes	THF	No	1.8 × 10 <sup>-8</sup> M	12
6	Tri-benzimidazolyl type	DMSO	Yes	0.284 μM	13
7	<b>Present work</b>	<b>CH<sub>3</sub>CN</b>	<b>Yes</b>	<b>4.63x10<sup>-8</sup> M</b>	

#### References:

1. SMART, SAINT, and XPREP; Siemens Analytical X-ray Instruments Inc.: Madison, WI, 1995.
2. G. M. Sheldrick, SADABS, Program for Area Detector Adsorption Correction, Institute for Inorganic Chemistry; University of Göttingen, Germany, 1996.
3. G. M. Sheldrick, Crystal structure refinement with SHELXL, *Acta Crystallogr. Sect. C: Struct. Chem.*, 2015, 71, 3.
4. R. Cariou, J. J. Chirinos, V. C. Gibson, G. Jacobsen, A. K. Tomov, G. J. P. Britovsek, and A. J. P. White, *Dalton Trans.*, 2010, 39, 9039–9045.
5. A. Jana, J. S. Kim, H. S. Jung, and P. K. Bharadwaj, A cryptand based chemodosimetric probe for naked-eye detection of mercury (II) ion in aqueous medium and its application in live cell imaging, *Chem. Commun.*, 2009, 4417–4419.
6. S. Sinha, B. Chowdhury, N. N. Adarsh, and P. Ghosh, A hexa-quinoline based C<sub>3</sub>-symmetric chemosensor for dual sensing of zinc(II) and PPI in an aqueous medium via chelation induced “OFF–ON–OFF” emission, *Dalton Trans.*, 2018, **47**, 6819–6830.

7. A. K. Mahapatra, P. Karmakar, J. Roy, S. Manna, K. Maiti, P. Sahoo, and D. Mandal, Colorimetric and ratiometric fluorescent chemosensor for fluoride ions based on phenanthroimidazole (PI): spectroscopic, NMR and density functional studies, *RSC Adv.*, 2015, **5**, 37935-37942.
8. S. Madhu and M. Ravikanth, Boron-dipyrrromethene based reversible and reusable selective chemosensor for fluoride detection, *Inorg. Chem.*, 2014, **53**, 1646 -1653.
9. A. Kushwaha, S. K. Patila, and D. Das, Pyrene-benzimidazole composed effective fluoride sensor: potential mimicking of a Boolean logic gate, *New J. Chem.*, 2018, **42**, 9200-9208.
10. I. S. Turan and E. U. Akkaya, Chemiluminescence Sensing of Fluoride Ions Using a Self-Immolative Amplifier, *Org. Lett.*, 2014, **16**, 1680–1683.
11. Y. Shen, X. Zhang, Y. Zhang, H. Li, and Y. Chen, An ICT-Modulated strategy to construct colorimetric and ratiometric fluorescent sensor for mitochondria-targeted fluoride ion in cell living, *Sens. Actuators B Chem.*, 2018, **258**, 544–549.
12. Y. Han, W. Yuan, H. Wang, M. Li, W. Zhang, and Y. Chen, Dual-responsive BN-embedded phenacenes featuring mechanochromic luminescence and ratiometric sensing of fluoride ions, *J. Mater. Chem. C*, 2018, **6**, 10456-10463.
13. Y. -C. Wu, J. -P. Huo, L. Cao, S. Ding, L.-Y. Wang, D. Cao, and Z. -Y. Wang, Design and application of tri-benzimidazolyl star-shape molecules as fluorescent chemosensors for the fast-response detection of fluoride ion, *Sens. Actuators B Chem.*, 2016, **237**, 865–875.